Natural brown adipose expansion and remission of hyperglycemia in obese SM/J mice

Caryn Carson[1,*], Mario A Miranda[1,*], Juan F Macias-Velasco[1], Subhadra Gunawardana[2], Jing Hughes[3], Sakura Oyama[1], Marcus Kunzmann[1], Heather Schmidt[1], Jessica P Wayhart[1], Heather A Lawson[1,#]

[1]Department of Genetics, Washington University School of Medicine, 660 South Euclid Ave, Saint Louis, MO, USA
[2]Department of Cell Biology and Physiology, Washington University School of Medicine, 660 South Euclid Ave, Saint Louis, MO, USA
[3]Department of Medicine, Washington University School of Medicine, 660 South Euclid Ave, Saint Louis, MO, USA

*Indicates co-first authors

[#]Corresponding author
660 South Euclid Ave
Campus Box 8232
Saint Louis, MO, 63110
ph: 314-362-7269, fax: 314-362-7855

Keywords: glycemic control, brown adipose, islets, obesity, metabolism, mouse model, transcriptome, extracellular matrix, cytokines

Summary

On a high fat diet, obese SM/J mice initially develop metabolic dysfunction, including impaired glucose tolerance and elevated fasting glucose. These abnormalities resolve spontaneously by 30 weeks of age despite persistence of obesity. The mice dramatically expand their brown adipose depots as they resolve glycemic dysfunction. They also expand their pancreatic islet populations and improve beta cell function. When the brown adipose depot is removed from normoglycemic high fat-fed mice, fasting blood glucose and glucose tolerance revert to unhealthy levels. This occurs naturally and spontaneously on a high fat diet, with no temperature or genetic manipulation. We identified 267 genes whose expression changes in the brown adipose when the mice resolve their unhealthy glycemic parameters, and find the expanded tissue has a 'healthier' expression profile. Understanding the physiologic and genetic underpinnings of this phenomenon in SM/J mice will open the door for innovative therapies aimed at improving glycemic control.

78 **Introduction**

79 An estimated 10-30% of obese individuals maintain glycemic control (Karelis, 2008) and some
80 longitudinal studies suggest their risk of developing type II diabetes is no greater than matched lean
81 individuals (Meigs et al., 2006). No causative factors underlying glycemic control in obesity have been
82 discovered, however the strongest predictors of impaired glycemic control in obesity are increased
83 visceral fat mass and adipose tissue dysfunction (Goossens, 2017; Klöting et al., 2010). Thus research
84 efforts have focused on understanding the genetic and physiological mechanisms of action of adipose
85 (Rosen and Spiegelman, 2014). Recent research reveals that brown adipose activity is associated with
86 anti-diabetic properties (Chechi et al., 2013; Cypess et al., 2009; Hanssen et al., 2016; van Marken
87 Lichtenbelt et al., 2009a; Saito, 2013; Saito et al., 2009; Stanford et al., 2013; Virtanen et al., 2009). Cold
88 exposure in both obese and lean individuals causes increased uptake of fatty acids and glucose into
89 brown adipose tissue, which is associated with an increase in total energy expenditure (van Marken
90 Lichtenbelt et al., 2009b; Ouellet et al., 2012; Saito et al., 2009). Further, increased brown adipose activity
91 has been shown to improve glucose homeostasis and insulin sensitivity in adults (Chondronikola et al.,
92 2014). The role of brown adipose in healthy metabolism is generally thought to be a function of its role in
93 non-shivering thermogenesis. However recent research indicates brown adipose also has a secretory
94 role, releasing adipokines into circulation that contribute to glycemic control, including fibroblast growth
95 factor 21 (FGF21) (Stanford et al., 2013) and neuregulin 4 (NRG4) (Wang et al., 2014). Transplantation
96 of brown adipose tissue into mouse models of both type I and type II diabetes greatly improves glucose
97 parameters, including fasting glucose levels and response to a glucose challenge (Gunawardana and
98 Piston, 2012, 2015), and this is thought to be due to brown adipose secreted factors (Villarroya et al.,
99 2017). Thus there is significant interest in identifying the brown adipokines responsible for these anti-
100 diabetic properties. While there are a variety of obese and diabetic mouse models, there are no mouse
101 models for understanding the relationship between brown adipose and glycemic control in obesity.

102 The SM/J inbred mouse strain has long been used for studying interactions between diet and
103 metabolism, and more recently has started to help uncover the genetic architecture underlying diet

104 induced obesity and glucose homeostasis (Cheverud et al., 2011; Lawson and Cheverud, 2010; Lawson
105 et al., 2010, 2011b, 2011a; Nikolskiy et al., 2015). It has previously been shown that fed a high fat diet,
106 SM/J mice display many of the characteristics of a diabetic-obese mouse: obesity, hyperglycemia,
107 glucose intolerance, and deficient insulin production at 20 weeks of age (Ehrich, 2003). Here, we report
108 that SM/J mice undergo a remarkable transformation between 20 and 30 weeks of age. Despite
109 persistence of the obese state, these mice enter into diabetic remission: returning to normoglycemia,
110 reestablishing glucose tolerance, and increasing insulin production without loss of insulin sensitivity.
111 Contemporary with this remission of glycemic parameters is a dramatic expansion of the interscapular
112 brown adipose depot. This study describes the morphological, physiological, and transcriptomic changes
113 that occur during this transition, and establishes the SM/J mouse as a unique model for understanding
114 the relationship between brown adipose and glycemic control in obesity. Understanding this relationship
115 in a natural model of glycemic resolution will set the stage for identifying novel, potentially therapeutic
116 targets for the improvement of glycemic control in obesity.
117
118 **Results**
119 *SM/J mice improve glucose parameters without weight loss*
120 The SM/J inbred mouse strain is used to explore dietary obesity and glycemic control (Lawson
121 and Cheverud, 2010). When fed a high fat diet (**Supplemental Table 1)**, SM/J mice develop obesity,
122 hyperglycemia, and impaired glucose tolerance by 20 weeks of age (Ehrich et al., 2003). We find that by
123 30 weeks of age, high fat-fed SM/J mice resolve their hyperglycemia and impaired glucose tolerance to
124 levels indistinguishable from low fat-fed controls, despite persistence of the obese state (**Figure 1A-D**).
125 Thirty-week-old high fat-fed SM/J mice experience a 2.5-fold increase in fasting insulin levels compared
126 to 20 week-old high fat-fed mice, and a 1.9-fold increase in fasting insulin compared to 30 week-old low
127 fat-fed mice (**Figure 1E**). This is reflected in a similar trend in total pancreatic insulin content (**Figure 1F**),
128 with no loss of insulin sensitivity, suggesting enhanced insulin secretion contributes to the resolution of
129 glucose parameters (**Figure 1G and H**).

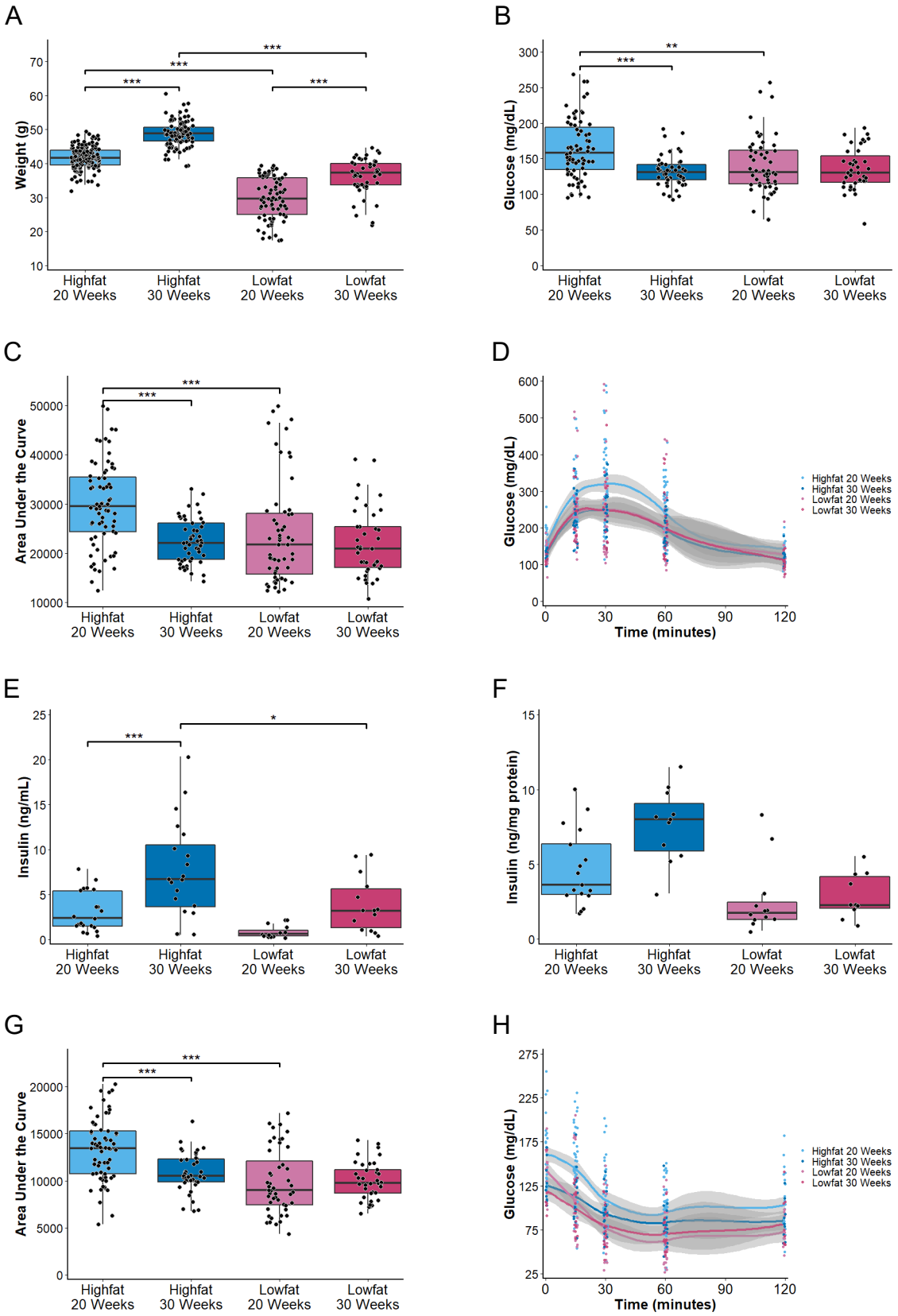
A
Weight (g)
Highfat 20 Weeks
Highfat 30 Weeks
Lowfat 20 Weeks
Lowfat 30 Weeks
B
Glucose (mg/dL)
C
Area Under the Curve
D
Glucose (mg/dL)
Time (minutes)
Highfat 20 Weeks
Highfat 30 Weeks
Lowfat 20 Weeks
Lowfat 30 Weeks
E
Insulin (ng/mL)
F
Insulin (ng/mg protein)
G
Area Under the Curve
H
Glucose (mg/dL)
Time (minutes)

131 **Figure 1. Obese SM/J mice improve glucose parameters between 20 and 30 weeks of age. A** High
132 fat-fed mice weigh significantly more than low fat-fed mice, and SM/J mice gain weight between 20 and
133 30 weeks of age on both diets, n = 48-131 mice per cohort. **B** 30 week-old high fat-fed mice have
134 significantly lower fasting glucose levels than at 20 weeks, which is no different than low fat-fed controls,
135 n = 22-47 mice per cohort. **C and D** 30 week-old high fat-fed mice have improved glucose tolerance
136 relative to 20 weeks, n = 22-47 mice per cohort. **E** Lower fasting glucose and improved glucose tolerance
137 corresponds with increased serum and **F** pancreatic insulin, n = 10-20 mice per cohort. **G and H** This
138 increase in insulin does not correspond to changes in insulin sensitivity in 30 week-old high fat-fed mice,
139 n = 22-47 animals per cohort. Equal numbers of males and females represented; * $p<0.05$, ** $p< 0.01$,
140 *** $p <0.001$
141

142 High fat-fed C57BL/6J mice also show a reduction in fasting glucose that is accompanied by
143 increased insulin with age (Ahren, 2004). However, the difference in circulating glucose between the high
144 fat- and low fat-fed controls remain significantly different over time. Moreover, high fat-fed C57BL/6J mice
145 show marked glucose intolerance that does not resolve with age. We observe a similar trend in the LG/J
146 strain of mice, where high fat-fed animals maintain higher fasting glucose levels and impaired glucose
147 tolerance relative to low fat-fed controls as they age (**Supplemental Figure 1**). The unique remission of
148 hyperglycemia and improved glucose tolerance observed in the high fat-fed SM/J strain indicates a
149 genetic basis.

150

151 *Increased islet cell replication underlies increased insulin production and improved islet function*

152 To understand the potential causes of the increased insulin secretion in high fat-fed SM/J mice,
153 we analyzed the morphology and function of pancreatic islets. The resolution of glucose parameters
154 correlates with increased pancreatic islet mass of high fat-fed mice at 30 weeks compared to 20 weeks
155 or to low fat-fed controls (**Figure 2A**). This increase in islet mass is driven by sustained mitosis of cells
156 within the islet, with a substantial increase in beta cell mass between 20 and 30 week high fat-fed mice
157 (**Figure 2B; Supplemental Figure 2**). A high fat diet and obesity are usually accompanied by a
158 progressive decline in beta cell function (Kahn et al., 2001; Da Silva Xavier, 2018), however a static
159 glucose-stimulated insulin secretion assay reveals that islets from high fat-fed SM/J mice improve insulin
160 secretion efficiency between 20 and 30 weeks, transitioning from non-glucose sensitive to glucose
161 sensitive (**Figure 2C**). Because high fat-fed SM/J islets are proliferative at 20 weeks, the non-existent

glucose-stimulated insulin secretion at 20 weeks suggests the nascent beta cells are not yet functionally mature (**Figure 2B and C**). This contrasts with high fat-fed C57Bl/6J mice, which have increased pancreatic islet size and reduced beta cell function (Roat et al., 2014), further underscoring the genetic basis of this phenomenon.

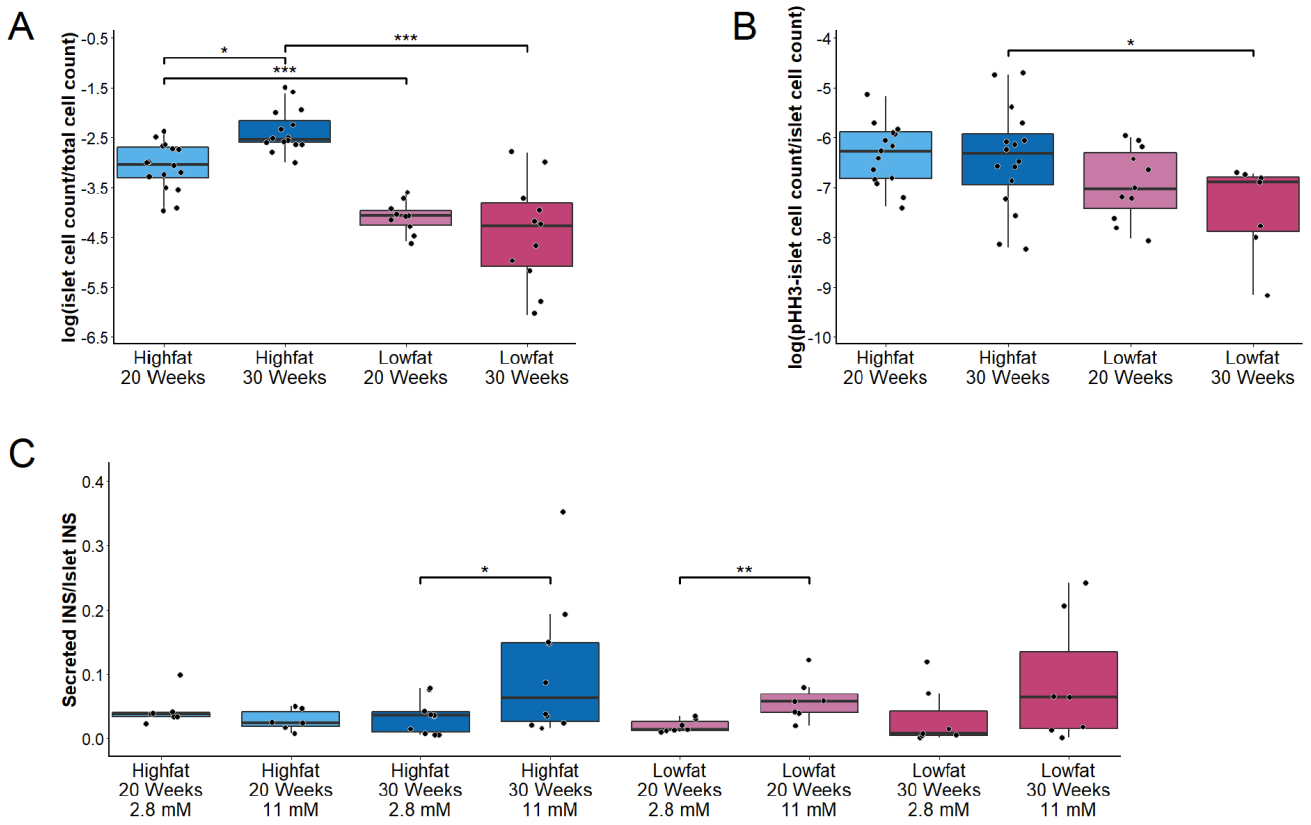

Figure 2. 30 week-old high fat-fed SM/J mice increase islet replication and improve insulin secretion. A Increased islet cell mass in high relative to low fat-fed mice, and in 30 relative to 20 week-old high fat-fed mice. **B** Islet cells in high fat-fed mice have elevated levels of phosphohistone-H3, a marker of mitosis. **C** Islets isolated from 30 week-old high fat-fed mice show restored insulin secretion capacity in the presence of high glucose compared to 20 week-old high fat-fed mice. Equal numbers of males and females represented, panels A and B: n = 12-16 mice per cohort; panel C: n = 6-8 mice per cohort; * $p<0.05$, ** $p< 0.01$, *** $p<0.001$

High fat-fed SM/J mice expand their interscapular brown adipose tissue depots

In conjunction with the resolution of glycemic parameters and improved insulin secretion, high fat-fed SM/J mice dramatically expand their interscapular brown adipose depots, which is not seen in low fat-fed control mice (**Figure 3A-C**). This has never been described in another mouse strain, and we do

179 not observe the phenomenon in the LG/J strain of mice on the same diets at any age (**Supplemental**
180 **Figure 3)**. To understand whether the tissue mass expansion is due to increased size of individual cells
181 or to increased number of total cells, we quantified adipocyte cell size and percent of phosphohistone-
182 H3 positive cells. There are no significant differences in average cell size in high fat-fed mice between
183 20 and 30 weeks, or relative to low fat-fed controls (**Supplemental Figure 4A**). Mice on both diets
184 undergo altered adipocyte area profiles between 20 and 30 weeks of age, however the low fat tissue
185 develops a profile significantly trending towards larger adipocytes at 30 weeks ($p=6.4^{-07}$) whereas the
186 high fat tissue develops a profile significantly trending towards smaller adipocytes at 30 weeks ($p=2.2^{-16}$)
187 (**Figure 3D and E**). This suggests that the expansion of the brown adipose depot in high fat-fed mice is
188 the result of increased proliferation of adipocytes, as newer adipocytes are smaller due to less lipid
189 accumulation. This is supported by quantification of brown adipose cells stained positive for the mitotic
190 marker phosphohistone H3, which trends towards higher mitosis in the brown adipose of high fat-fed
191 animals (**Supplemental Figure 4B**).

192 Obesity has been associated with structural and functional "whitening" of brown adipose depots
193 in rodents (Lapa et al., 2017; Roberts-Toler et al., 2015; Shimizu and Walsh, 2015; Shimizu et al., 2014).
194 Histological analysis of the fat depot taken from high fat-fed SM/J mice at 30 weeks of age confirms the
195 adipocytes in this expansion are brown adipocytes, with small multilocular lipid droplets and high UCP1
196 staining (**Supplemental Figure 5**). Expression of canonical brown adipose genes *Ucp1* and *Cidea* do
197 not change between 20 and 30 weeks (**Figure 3F-G).** Further, expression of *Tbx1*, a marker specific for
198 beige adipocytes (Wu et al., 2012), indicates that neither brown nor white adipose is "beiging" (**Figure**
199 **3H**). Finally, there is no significant difference in brown adipose tissue mitochondrial content between the
200 diets or ages (**Figure 3I**). There is no difference in core body temperature or circulating free fatty acids
201 between high and low fat-fed cohorts or between 20 and 30 weeks of age (**Supplemental Figure 6A**
202 **and B**). Additionally, while there are diet-dependent differences in the catecholamines norepinephrine
203 and epinephrine, which activate UCP1-mediated leak respiration and non-shivering thermogenesis, there
204 is no change in levels between ages in the high fat-fed mice (**Supplemental Figure 6C and D**). Thus,

205 the interscapular adipose depot in high fat-fed SM/J mice maintains a brown adipose identity after
206 expansion that is not dependent on whole-animal beiging, and is also not associated with altered
207 thermogenesis.

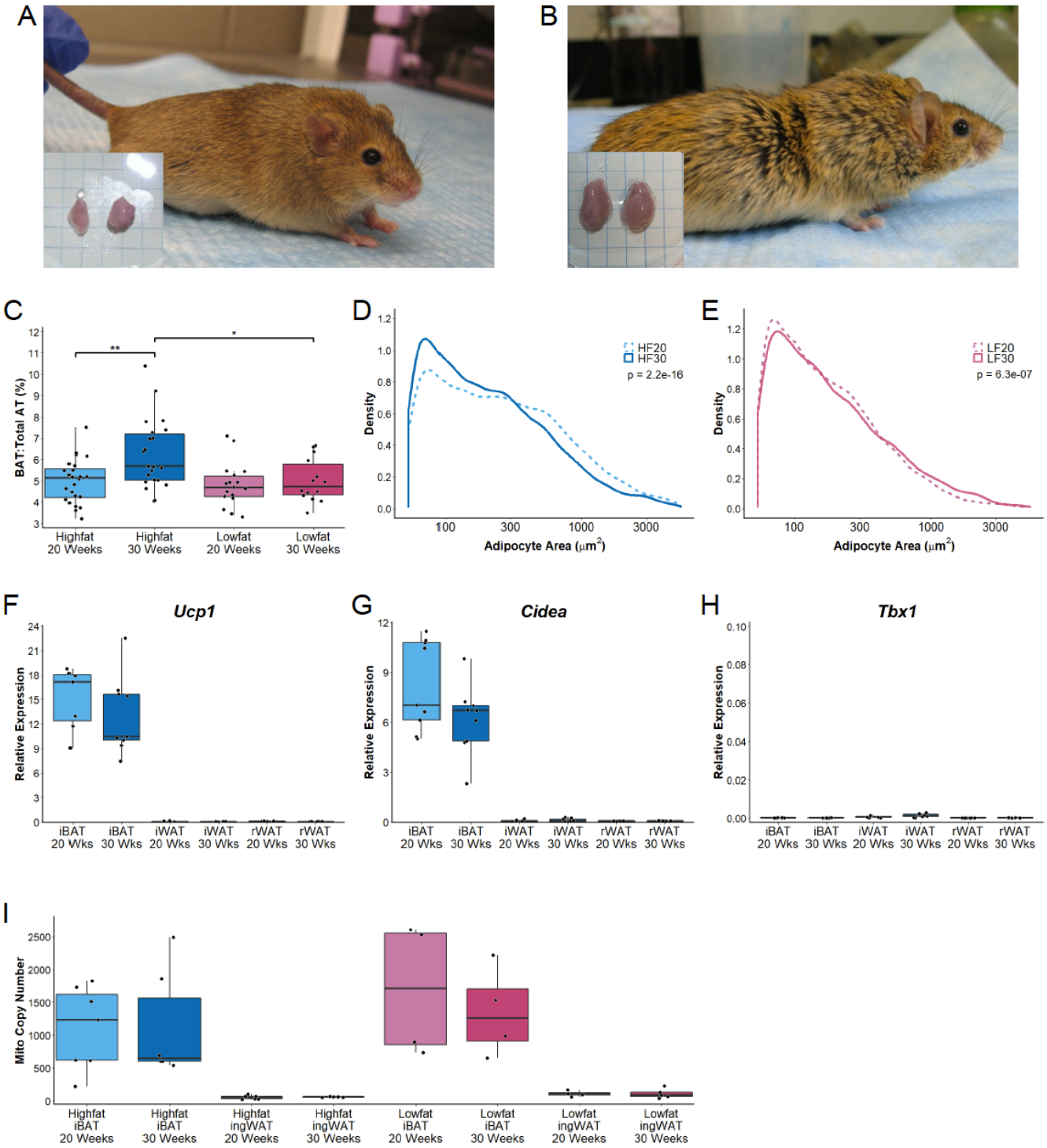

208

209 **Figure 3. Brown adipose expansion in 30 week-old high fat-fed SM/J mice.** Representative pictures
210 of **A** 20 week and **B** 30 week-old high fat-fed female mice. **C** Quantification of interscapular brown adipose
211 depot as a proportion of total fat mass, n = 16-25 mice per cohort. **D and E** Cell area density graphs for
212 high fat and low fat-fed cohorts. Data are plotted on a log10 scale for visualization, n = 4 mice per cohort.
213 **F-H** Gene expression levels quantified in three adipose depots of high fat-fed mice: interscapular brown
214 adipose (iBAT), inguinal white adipose (ingWAT), and reproductive white adipose (repWAT), n = 6-10
215 mice per cohort and tissue. Canonical brown adipose genes (**F)** *Ucp1* and (**G)** *Cidea* show high
216 expression in iBAT and no difference between 20 and 30 week-old mice. Beige adipose marker (**H)** *Tbx1*
217 is not expressed in any depot. **I** Mitochondrial copy number was significantly higher in brown adipose
218 tissue than in inguinal white adipose tissue at both 20 and 30 week time points with no significant
219 difference between high or low fat-fed mice, n = 6-7 mice per cohort and tissue. Equal numbers of males
220 and females represented. * $p<0.05$, ** $p< 0.01$
221

222 *RNA sequencing reveals enrichment of differentially expressed cytokines and genes affecting extra*
223 *cellular matrix*

224 Since the brown adipose tissue expansion is unique to high fat-fed SM/J mice, we anticipated that
225 there would be corresponding unique transcriptomic changes in the brown adipose. Indeed, we identified
226 267 genes whose expression significantly and uniquely changes between 20 and 30 weeks of age in
227 high fat-fed SM/J brown adipose tissue (at a 5% FDR, out of 13,253 total genes expressed;
228 **Supplemental Table 2**). These expression changes occur when the mice resolve their unhealthy
229 glycemic parameters and expand their brown adipose depots. These genes are not differentially
230 expressed in white adipose tissue taken from the same animals or in low fat-fed SM/J controls (**Figure**
231 **4A**). Additionally, they are not differentially expressed in the LG/J strain of mouse, again underscoring
232 the genetic basis of the phenomenon (**Supplemental Figure 7; Supplemental Table 3**).

233 Over-representation analysis indicates these genes are enriched for those involved in cytokine-
234 cytokine receptor interactions ($p=3.23e^{-06}$), signaling receptor activity ($p = 5.70e^{-06}$), cell surface receptor
235 signaling ($p=2.04e^{-07}$), and extracellular matrix components ($p = 7.93\ e^{-13}$), among others (**Figure 4B;**
236 **Supplemental Table 4**). These are intriguing results because brown adipose has been identified as a
237 source of cytokines that influence beta cell health and glucose homeostasis (Villarroya et al., 2017; Wang
238 et al., 2015), and extracellular matrix changes are essential for tissue expansion, cellular signaling, and
239 regulation of growth factor bioavailability (Frantz et al., 2010).

240 Several genes belonging to these biological categories have evidence for their involvement in
241 glucose homeostasis and change expression in a direction that is associated with improved metabolic
242 health in high fat-fed SM/J mice between 20 and 30 weeks of age (**Figure 4C**). In particular, the direction
243 of expression change reveals that the expansion of brown adipose is associated with a decrease in
244 inflammatory (e.g. interleukin 7 receptor, *Il7r*) (Kim et al., 2014) and fibrotic markers (e.g. collagen type
245 VIII alpha 1 chain, *Col8a1*; semaphorin 3C, *Sema3c*) (Mejhert et al., 2013; Sun et al., 2013), and changes
246 in extracellular matrix components (e.g. matrix metallopeptidase 12, *Mmp12*; procollagen c-
247 endopeptidase enhancer, *Pcolce*) (Huang et al., 2011; Lee et al., 2014) and cytokine activity (e.g.
248 coagulation factor VII, *F7*; leptin, *Lep*; secreted frizzled-related protein 1, *Sfrp1*) (D'souza et al., 2017;
249 Edén et al., 2015; Gauger et al., 2013) (**Supplemental Figure 8**). Other mouse models of diet-induced
250 obesity develop unhealthy brown adipose transcriptomes characterized by increased expression of pro-
251 inflammatory genes and fibrotic markers (McGregor et al., 2013; Alcalá et al., 2017). The direction of
252 expression change in our brown adipose tissue supports the uniqueness of the high fat-fed SM/J mice.

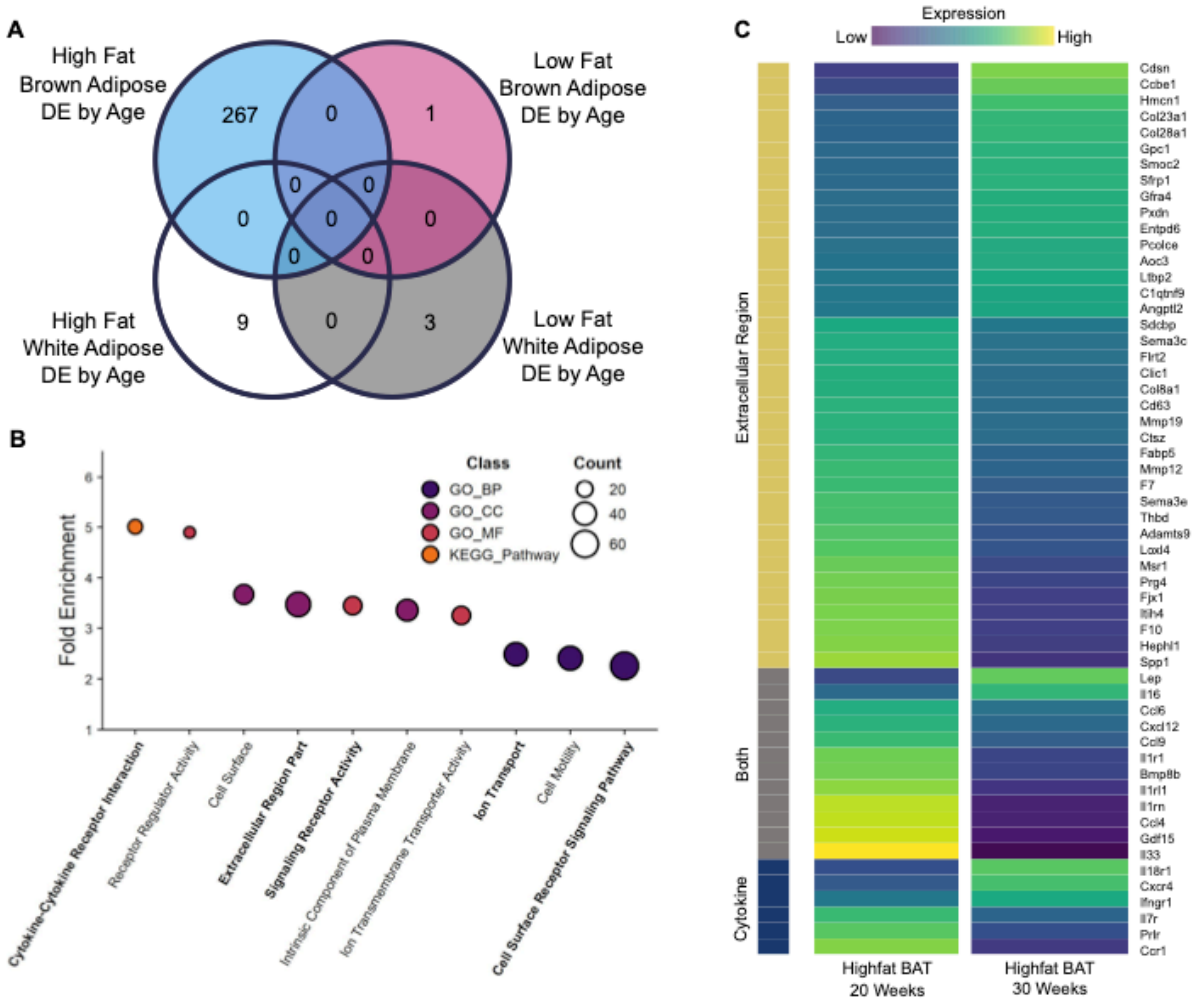

Figure 4. High fat-fed SM/J mice have unique brown adipose differential expression between 20 and 30 weeks of age. A Venn diagram illustrating the number of genes differentially expressed between high and low fat-fed 20 and 30 week-old SM/J interscapular brown or reproductive white adipose tissues. No genes are differentially expressed in more than one diet-by-tissue cohort. **B** Enriched terms colored by class (Gene Ontology Biological Process (GO_BP), Cellular Component (GO_CC), Molecular Function (GO_MF), and KEGG Pathway. **C** Heatmap of differentially expressed brown adipose tissue genes between high fat-fed 20 and 30 week-old mice belonging to cytokine, extracellular matrix, or both gene ontologies. Equal numbers of males and females represented, n = 8 animals per age-by-diet cohort.

30 week old high fat-fed SM/J brown adipose has a healthier co-expression profile

Because variation in glucose homeostasis is complex and the result of many interacting genes, we examined the co-expression profile of genes belonging to the enriched cytokine and extracellular matrix (ECM) biological categories (**Figure 4B and C**). We find that the structure of the differentially expressed ECM and cytokine genes is significantly different between 20 and 30 week-old high fat-fed

268 animals (p=0.01). To determine if the co-expression structure of these genes in 30 week-old high fat-fed
269 animals' brown adipose is more similar to the 20 week-old high fat-fed or to the low fat-fed animals', we
270 compared the overall co-expression correlation structure between the diet and age cohorts for these
271 genes. Remarkably, we find the 30 week-old high fat-fed small brown adipose ECM and cytokine co-
272 expression profile is most similar to the 20 week-old low fat-fed animals' (probability of difference between
273 high fat-fed 30 weeks and low fat-fed 20 weeks = 0.07; probability of difference between high fat-fed 30
274 weeks and low fat-fed 30 weeks = 0.04) (**Figure 5A**). Thus, the brown adipose cytokine and ECM gene
275 co-expression profile appears 'healthier' in 30 week-old high fat-fed animals after expansion and
276 remission of the diabetic phenotype. This is illustrated in **Figure 5B**.

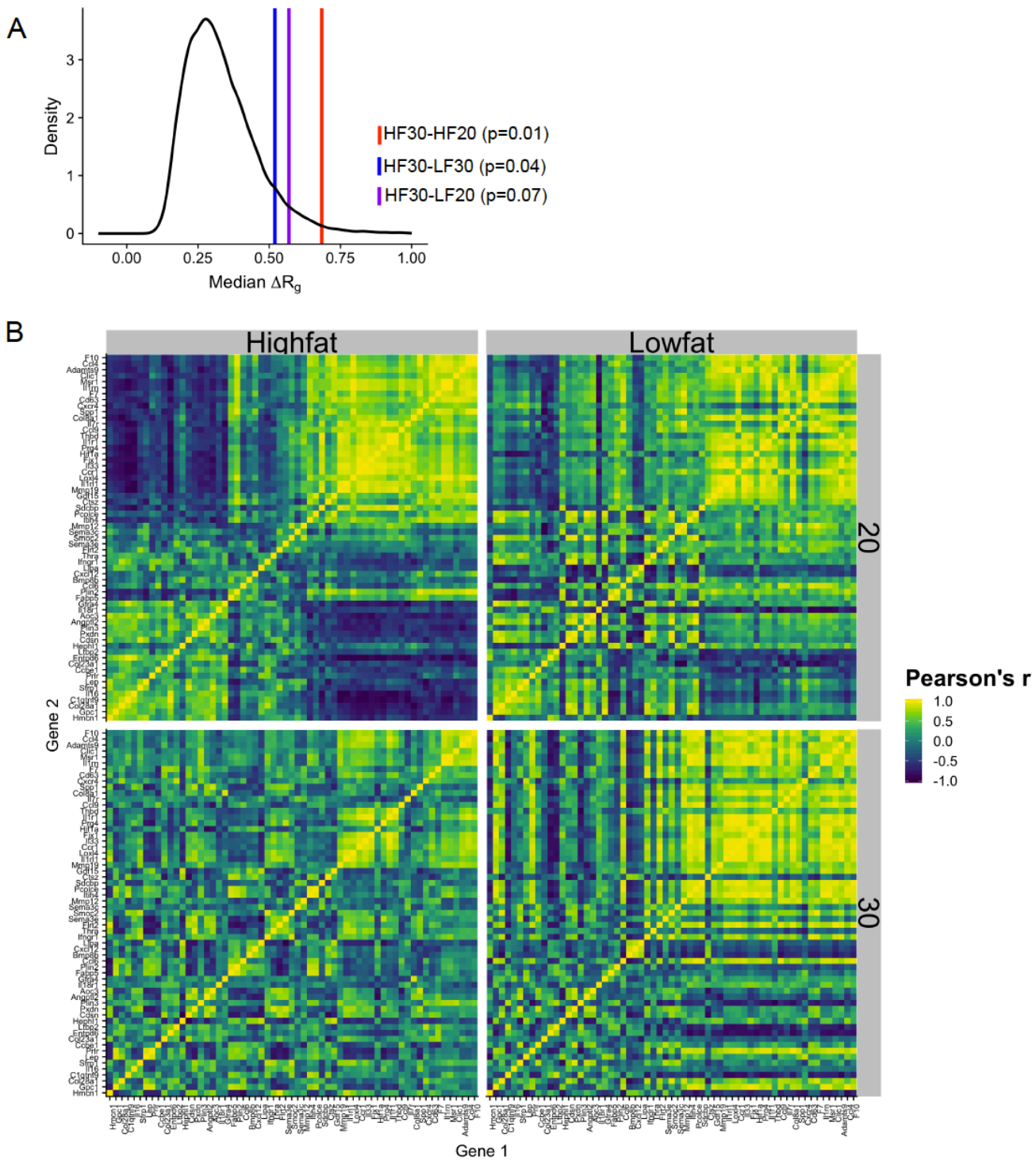

Figure 5. High fat-fed 30 week-old SM/J mice have a cytokine and ECM gene co-expression profile most similar to low fat-fed 20 week-old mice. A The median change in correlation structure is plotted as a vertical line against the null model. High fat-fed 30 week-old SM/J mice have a co-expression profile significantly different from high fat-fed 20 week-old SM/J mice, and not significantly different from low fat-fed 20 week-old mice. **B** Heatmap of the gene expression correlation matrices for each cohort. HF30 = high fat-fed 30 week-old; HF20 = high fat-fed 20 week-old; LF30 = low fat-fed 30 week-old; LF20 = low

284 fat-fed 20 week-old. Equal numbers of males and females represented, n = 8 animals per age-by-diet
285 cohort.
286

287 *Glucose parameters revert to an unhealthy state in SM/J mice when the brown adipose depot is removed*

288 If the brown adipose expansion is directly related to the glycemic resolution of the high fat-fed
289 SM/J mice, removing that expansion should revert the glucose parameters to their unhealthy state. To
290 test this, we removed the interscapular brown adipose depots from normoglycemic 30 week-old mice.
291 After recovery, at 35 weeks of age, we measured basal glucose levels and performed a glucose tolerance
292 test. We find that glucose parameters revert to unhealthy, 20 week-old measurements when the brown
293 adipose depot is removed (**Figure 6 A-B**), indicating that the expanded brown adipose tissue is
294 necessary for the observed remission of unhealthy glycemic parameters in high fat-fed SM/J mice.

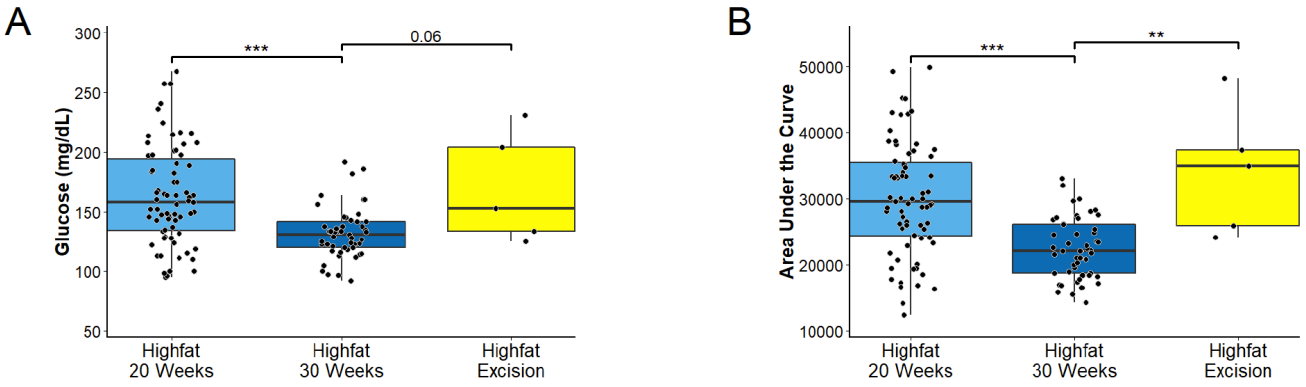

295

296 **Figure 6. Glycemic parameters revert to unhealthy levels when the brown adipose depot is**
297 **removed. A** Blood glucose assessed after a 4 hour fast. **B** A glucose tolerance test indicates that glucose
298 tolerance is reduced after the brown adipose depot is removed. n = 5 excision animals, representing 4
299 males and 1 female.
300

301 **Discussion**

302 Obesity (body-mass index [BMI] ≥30 kg.m^2) is associated with serious metabolic complications,
303 including type II diabetes, cardiovascular disease, cancer, and stroke (Abdullah et al., 2010; Kenchaiah
304 et al., 2002; Rauscher et al., 2000; Reeves et al., 2007; Strazzullo et al., 2010). Currently, 38% of
305 American adults are classified as obese (Flegal et al., 2016), 9.4% have type II diabetes, and an
306 additional 34% are pre-diabetic, costing 327 billion dollars in annual medical costs (Centers for Disease

307 Control and Prevention, 2017; Yang et al., 2018). Obesity and diabetes are tightly linked; obesity raises
308 the risk of developing type II diabetes 27—76 fold, while approximately 60% of diabetics are obese
309 (Abdullah et al., 2010; Centers for Disease Control and Prevention, 2017; Chatterjee et al., 2017; Colditz
310 et al., 1995). The obesity-diabetes axis centers on glycemic control, where excess caloric intake and
311 body fat demands increased beta cell insulin secretion to maintain normoglycemia. In many individuals,
312 the prolonged obese state results in insulin resistance, beta cell death, loss of insulin production, and
313 chronic hyperglycemia. Though weight loss is *the* gold standard for treating glycemic dysfunction in
314 obesity, many obese people are unable to achieve long-term weight loss (Dulloo and Montani, 2015;
315 Tomiyama et al., 2013). Currently, metformin and thiazolidinediones are prescribed to prevent the
316 development of diabetes in obese individuals, but pharmacological therapy has been shown to have only
317 modest protective effects (Chatterjee et al., 2017; Nathan et al., 2015). Greater understanding of the
318 relationship between obesity and glycemic control is needed to develop more effective preventative
319 measures for obese patients.

320 Here we describe morphological, physiological, and transcriptomic changes that occur during
321 brown adipose expansion and remission of hyperglycemia in SM/J mice. The SM/J strain was derived
322 from a pool of seven inbred strains and selected for small body size at 60 days (Beck et al., 2000;
323 MacArthur, 2002; Nikolskiy et al., 2015). The strain has been used extensively in genetic studies of
324 complex traits related to growth and metabolism (Kenney-Hunt et al., 2006; Lawson et al., 2010, 2011a,
325 2017; Norgard et al., 2011), particularly because SM/J mice are strongly responsive to high fat diet-
326 induced obesity. These studies all used mice aged 20 weeks or less, when SM/J's develop the classic
327 hallmarks of obese-diabetic mice. We discovered that by 30 weeks of age, coinciding with a dramatic
328 expansion of interscapular brown adipose tissue, their hyperglycemia, impaired glucose tolerance, and
329 deficient insulin secretion in response to glucose stimulation goes into remission despite persistence of
330 obesity. Dissecting the genetic basis of this phenomenon has the potential to uncover novel relationships
331 among brown adipose, glucose homeostasis, and obesity.

332 We identified 267 genes whose expression significantly and uniquely changes between 20 and
333 30 weeks of age in high fat-fed SM/J brown adipose tissue. We hypothesize that these genes affect
334 brown adipose function and contribute to the phenomenon we observe. The expression changes occur
335 when the mice resolve their unhealthy glycemic parameters and expand their brown adipose depots.
336 These genes are not differentially expressed in white adipose tissue taken from the same animals. These
337 genes are not differentially expressed between low fat-fed intra-strain controls at the same ages or in a
338 unique mouse strain that does not resolve glycemic parameters or expand brown adipose tissue. Further,
339 30 week-old high fat-fed SM/J brown adipose has an overall 'healthier' expression profile, supported by
340 the analysis of the correlation structure among the age-by-diet cohorts for cytokines and ECM genes
341 (**Figure 5A**).

342 We focus on genes associated with ECM and cytokine activity because both biological categories
343 are enriched in the set of genes that significantly change expression in brown adipose during the
344 remission of glycemic parameters. Brown adipose is a source of endocrine signals with anti-diabetic
345 properties (Stanford et al., 2013; Wang et al., 2014) and is involved in extensive cross-talk with other
346 organs (Poekes et al., 2015). It secretes cytokines that influence whole-body glucose homeostasis and
347 insulin sensitivity including IGF1, FGF21, NRG-3 and NRG-4 (Kajimura et al., 2015; Wang et al., 2015).
348 ECM changes are essential for cellular signaling, regulation of growth factor bioavailability, and
349 accompany healthy adipose expansion. However, extreme changes in ECM protein levels are associated
350 with adipose dysfunction in obesity; thus a fine balance between tissue remodeling and excessive
351 accumulation of ECM proteins must be achieved to maintain adipose tissue homeostasis (Hasegawa et
352 al., 2018; Sun et al., 2013).

353 We highlight 8 cytokines and ECM genes that significantly change expression in a direction
354 associated with improved metabolic health in previous studies. *Il7r*, which was found to be one of the
355 highest ranking genes in the white adipose tissue inflammatory response pathway (Moreno-Viedma et
356 al., 2016b), decreases expression between 20 and 30 weeks of age in high fat-fed SM/J brown adipose.
357 *Col8a1* and *Sema3C* are both associated with adipose tissue fibrosis (Hasegawa et al., 2018; Mejhert et

358 al., 2013). Increased adipose tissue fibrosis is a signature of dysfunctional adipose and is associated with
359 impaired glucose homeostasis and insulin resistance (Sun et al., 2013). Both *Col8a1* and *Sema3c*
360 expression decrease between 20 and 30 weeks in high fat-fed SM/J brown adipose. *Mmp12* is an enzyme
361 that contributes to adipose tissue remodeling (Maquoi et al., 2002). Increased *Mmp12* expression is
362 associated with white adipose tissue inflammation and insulin resistance and *Mmp12*$^{-/-}$ mice are more
363 insulin sensitive than wildtype controls on a high fat diet (Lee et al., 2014). Its expression decreases in
364 30 week old high fat-fed SM/J brown adipose. *Pcolce* encodes a glycoprotein that regulates collagen
365 processing at the ECM (Raz et al., 2013). Mice with defects in ECM collagen are glucose intolerant,
366 hyperglycemic, and insulin resistant (Huang et al., 2011). PCOLCE is one of 15 key drivers that
367 collectively account for 22% of GWAS hits for type II diabetes in a recent multiethnic meta-analysis (Shu
368 et al., 2017). *Pcolce* expression is significantly increased in 30 week old high fat-fed SM/J brown adipose.
369 *F7*, *Lep*, and *Sfrp1* are each secreted proteins. Increased *F7* plays a role in the pathogenesis of obesity
370 (Takahashi et al., 2015). In particular it has been shown to induce beta cell death and impaired islet
371 glucose-stimulated insulin secretion (Edén et al., 2015). Increased *Lep* can dramatically lower blood
372 glucose levels in diabetic rodent models (D'souza et al., 2017). In brown adipose, leptin has been shown
373 to stimulate glucose uptake (Denroche et al., 2016). *Sfrp1* is dysregulated in obesity and *Sfrp1*$^{-/-}$ mice
374 have elevated blood glucose and impaired glucose tolerance when fed a high fat diet (Gauger et al.,
375 2013; Lagathu et al., 2010). *F7* expression is decreased and *Lep* and *Sfrp1* are increased in 30 week old
376 high fat-fed SM/J brown adipose tissue. Most of what is known about the role of these 8 genes in adipose
377 comes from studies of white adipose tissue, but none of these genes are differentially expressed in SM/J
378 white adipose. Many additional genes likely contribute to the observed phenomenon, however little, if
379 anything, is known about their role in brown adipose tissue. The 267 differentially expressed genes we
380 identified represent a set of actionable candidates for further functional studies of their role in brown
381 adipose and glucose homeostasis.

382 There is great interest in harnessing the potential of brown adipose to treat obesity and diabetes,
383 either through the calorie burning action of non-shivering thermogenesis or the endocrine action of

384 adipokines. Research into the effects of brown adipose on systemic metabolism is in its infancy, and the
385 community needs appropriate animal models to interrogate its physiological roles and identify potentially
386 druggable targets. We present the SM/J mouse strain as a unique model to address this need. High fat-
387 fed obese SM/J mice revert to normoglycemic at 30 weeks of age. High fat-fed normoglycemic SM/J mice
388 have dramatically expanded brown adipose depots and improved islet glucose-stimulated insulin
389 secretion. When the brown adipose depot is removed from normoglycemic high fat-fed SM/J mice, fasting
390 blood glucose and glucose tolerance revert to unhealthy levels. This occurs naturally and spontaneously
391 on a high fat diet, with no temperature or genetic manipulation. To our knowledge this has never been
392 described in another mouse strain and our transcriptomic studies indicate the phenomenon is genetic.
393 The SM/J mouse provides a tractable system in which to understand the relationship between brown
394 adipose and glycemic control in obesity. Understanding this relationship in the SM/J mouse will open
395 doors for identifying novel, potentially druggable targets for the improvement of glycemic control in
396 humans.
397
398 **Methods**
399 *Animal Husbandry and Phenotyping*
400 SM/J and LG/J mice were obtained from The Jackson Laboratory (Bar Harbor, ME). Experimental
401 animals were generated at the Washington University School of Medicine and all experiments were
402 approved by the Institutional Animal Care and Use Committee in accordance with the National Institutes
403 of Health guidelines for the care and use of laboratory animals. Pups were weaned at 3 weeks and reared
404 in same-sex cages of 3-5 animals until necropsy. At weaning, mice were randomly placed on a high fat
405 diet (42% kcal from fat; Teklad TD88137) or an isocaloric low fat diet (15% kcal from fat; Research Diets
406 D12284) (**Supplemental Table 1**). Feeding was *ad libitum*. The animal facility operates on a 12 hour
407 light/dark cycle with a constant ambient temperature of 21°C. Animals were weighed weekly until
408 sacrifice. At 18 and 28 weeks of age, animals were subject to an intraperitoneal glucose tolerance test
409 after a 4 hour fast. At 19 and 29 weeks of age animals were subject to an intraperitoneal insulin tolerance

410 test. At 20 or 30 weeks of age, body composition was determined by MRI and temperature was measured
411 with a rectal thermometer. After a 4 hour fast, at 20 or 30 weeks of age, animals were given an overdose
412 of sodium pentobarbital and blood was collected via cardiac puncture. Euthanasia was achieved by
413 cardiac perfusion with phosphate-buffered saline. After cardiac perfusion, tissues were collected and
414 flash frozen in liquid nitrogen and stored at -80°C, or processed according to protocols for histology and
415 other assays.
416
417 *Blood plasma assays*
418 Fasting blood glucose was measured using a GLUCOCARD Vital glucometer (Arkay, MN USA).
419 ELISAs measuring plasma levels of insulin (ALPCO 80-INSMR-CH01) and free fatty acids (Wako Life
420 Sciences 995-34693) were quantified according to manufacturer's protocol. Catecholamines were
421 assayed through the Vanderbilt University Medical Center's Hormone Assay and Analytical Services
422 Core (www.vumc.org/hormone/assays; NIH grants DK059637 (MMPC) and DK020593 (DRTC)).
423
424 *Pancreatic insulin content*
425 Whole pancreas was homogenized in acid ethanol and incubated at 4°C for 48 hours, shaking.
426 Homogenate was centrifuged at 2500 rpm for 30 min at 4°C. Supernatant was collected and stored at -
427 20°C. Protein content was measured using Pierce BCA Protein Assay kit (Thermo Scientific) according
428 to manufacturer's instructions, and read at 562 nm on the Synergy H1 Microplate Reader (Biotek). Insulin
429 content was measured with ALPCO ultrasensitive Insulin ELISA (ALPCO 80-INSMR-CH01) according to
430 manufacturer's instructions.
431
432 *Glucose-stimulated insulin secretion*
433 Pancreas was removed and placed in 8mL HBSS buffer on ice. Pancreas was then thoroughly
434 minced. 120mg Collagenase P (Roche) was dissolved in HBSS and aliquoted into 20 x 500ul tubes. One
435 tube (500ul) was added to the minced pancreas in 8ml HBSS. Mixture was then shaken in a 37°C water

436 bath for 12 minutes. Mixture was spun at 2000 rpm for 1 minute. The pellet was washed twice with HBSS,
437 spinning in between. The pellet was re-suspended in HBSS and transferred a petri dish. Hand-selected
438 islets where placed in sterile-filtered RPMI with 11mM glucose, 5% pen/strep, and 10% Fetal Bovine
439 Serum. Islets were rested overnight in a cell culture incubator set to 37°C with 5% C02. The following
440 day, islets were equilibrated in KRBH buffer containing 2.8 mM glucose for 30 minutes at 37°C. 5 Islets
441 were hand selected and placed in 150ul KRBH containing either 2.8 or 11mM glucose. Tubes were placed
442 in a 37°C water bath for 45 min. Islets were then spun at 2000RPM, hand-picked with a pipette, and
443 transferred from the secretion tube and placed in the content tube with acid ethanol. The content and
444 secretion tubes were stored at -20°C overnight. Each condition was performed in duplicate for each
445 individual.

446 ALPCO Ultrasensitive ELISA (80-INSMU-E01) was performed according to manufacturer's
447 instructions, with the secretion tubes diluted 1:5, and content tubes diluted 1:100. Normalized insulin
448 secretion was calculated by dividing the secreted value by the content value. Glucose stimulated insulin
449 secretion was calculated by dividing the normalized insulin secretion at 11mM by the normalized insulin
450 secretion at 2.8mM. Each sample was measured in duplicate.

451

452 *Islet histology and analyses*

453 At the time of tissue collection, whole pancreas was placed in 3 mL of neutral buffered formalin.
454 These samples were incubated at 4C while gently shaking for 24 hours. Immediately afterwards, samples
455 were placed into plastic cages and acclimated to 50% EtOH for 1 hour. Samples were then processed
456 into paraffin blocks using a Leica tissue processor with the following protocol: 70% EtOH for 1 hour x 2,
457 85% EtOH for 1 hour, 95% EtOH for 1 hour x 2, 100% EtOH for 1 hour x 2, Xylenes for 1 hour x 2, paraffin
458 wax. Pancreas blocks were sectioned into four sections 4 μm thick at least 100 μm from each other.

459 Slides were incubated at 60C for 1 hour, then placed in xylenes to remove remaining paraffin wax.
460 Slides were then rehydrated using successive decreasing EtOH concentrations (xylenes x 2, 50% EtOH

461 in xylenes, 100% EtOH x 2, 95% EtOH, 70% EtOH, 50% EtOH, H2O). Slides were incubated in sodium
462 citrate (pH 6) at 85C for 30 minutes, then submerged in running water for 5 minutes. Slides were washed
463 with 0.025% Triton X-100 in TBS and blocked in 10% normal donkey serum for 1 hour (Abcam ab7475),
464 followed by incubation with primary antibody overnight at 4C. [Primary antibodies: rat anti-insulin (1:100,
465 R&D MAB1417), mouse anti-glucagon (1:100, abcam ab10988), and rabbit anti-phospho-histone H3
466 (1:100, Sigma SAB4504429)]. After an additional wash, secondary antibody was applied for 1 hour at
467 room temperature. [Secondary antibodies: donkey anti-rabbit 488 (1:1000, abcam ab150061), donkey
468 anti-mouse 647 (1:1000, abcam ab150107), and donkey anti-rat 555 (1:1000, abcam ab 150154)].
469 Fluoroshield Mounting Medium with DAPI (Abcam) was applied to seal the coverslip and slides were
470 stored at 4C. Imaging was performed using the Zeiss AxioScan .Z1 at 20X magnification and 94.79%
471 laser intensity.

472 Background was subtracted from DAPI, insulin, glucagon, and PHH3 channels using ImageJ.
473 DAPI channel was used to identify total nuclei in CellProfiler. Insulin and glucagon channels were
474 combined and overlaid on the DAPI image to identify islet nuclei. Islet nuclei images were overlaid with
475 PHH3 stain to identify mitotic islet nuclei. Total nuclei, islet nuclei, and mitotic nuclei were summed across
476 all 4 slides for each individual, 12-16 individuals per cohort. Islet mass is reported as islet nuclei divided
477 by total nuclei. Mitotic islet index is reported as mitotic islet nuclei divided by islet nuclei.

478

479 *Brown adipose histology*

480 At the time of tissue collection, small portions of interscapular brown and reproductive white
481 adipose tissues were placed in 1 mL of neutral buffered formalin. These samples were incubated at 4C
482 while gently shaking for 24 hours. Immediately afterwards, samples were placed into plastic cages and
483 processed into paraffin blocks using a Leica tissue processor with the following protocol: 70% EtOH for
484 1 hour x 2, 85% EtOH for 1 hour, 95% EtOH for 1 hour x 2, 100% EtOH for 1 hour x 2, Xylenes for 1 hour
485 x 2, paraffin wax. Adipose blocks were sectioned into 6 μm sections, with 2-4 slices on each slide.

486

487 *H&E Staining*

488 Slides were incubated at 60C for 1 hour, then placed in xylenes to remove remaining paraffin wax.
489 Slides were then rehydrated using successive decreasing EtOH concentrations (xylenes x 2, 100% EtOH
490 x 2, 95% EtOH, 70% EtOH, H2O). Slides were incubated in hematoxylin (Leica Surgipath 3801570),
491 Define (3803590), Blue Buffer 8 (3802915), and eosin (3801616), and dehydrated (95% EtOH, 100%
492 EtOH, xylene x 2). Imaging was performed using the Zeiss AxioPlan2 microscope and Olympus DP
493 software. Analysis of adipocyte size was performed using ImageJ. Images were converted to black and
494 white and skeletonized to reveal only the cell wall outlines. Cell area was calculated from outlines with a
495 lower limit of 50 um and upper limit of 700 um to reduce noise. All cells from a cohort (4-7 images each
496 from 4 animals per cohort, equal numbers of males and females) were pooled for cell area density
497 analysis. A Welch's unequal variances t-test was performed between ages in each diet to determine
498 significant differences.

499

500 *Immunofluorescence*

501 Slides were incubated at 60C for 1 hour, then placed in xylenes to remove remaining paraffin wax.
502 Slides were then rehydrated using successive decreasing EtOH concentrations (xylenes x 2, 50% EtOH
503 in xylenes, 100% EtOH x 2, 95% EtOH, 70% EtOH, 50% EtOH, 0.3% H2O2 in MeOH, H2O). Slides were
504 washed with TBS and blocked in 10% normal donkey serum (Abcam ab7475) for 1 hour, followed by
505 incubation with primary antibody overnight at 4C. [Primary antibodies: rabbit anti-Ucp1 (1:100, Sigma
506 U6382) and mouse anti-PHH3 (1:100, Invitrogen MA5-15220)]. After an additional wash, secondary
507 antibody was applied for 1 hour at room temperature [Secondary antibodies: donkey anti-rabbit 488
508 (1:1000, Abcam ab150061) and donkey anti-mouse 647 (1:200, Abcam ab150107)]. Fluoroshield
509 Mounting Medium with DAPI (Abcam) was applied to seal the coverslip and slides were stored at 4C.

510 Imaging was performed using the Zeiss Confocal microscope and Zen Lite imaging program. PHH3
511 analysis was performed using the CellProfiler program. Background was subtracted from DAPI and PHH3
512 channels using ImageJ. DAPI channel was used to identify total nuclei in CellProfiler. Adipose nuclei
513 images were overlaid with PHH3 stain to identify mitotic adipose nuclei. Mitotic nuclei were summed
514 across all 4 slides for each individual. Mitotic adipose index is reported as mitotic adipose nuclei divided
515 by adipose nuclei multiplied by 100%.

516

517 *Quantitative rt-PCR*

518 Total RNA was extracted from brown, inguinal, and reproductive adipose samples using the
519 Qiagen RNeasy Lipid Kit. High-Capacity cDNA Reverse Transcription Kit (Thermofisher) was used for
520 reverse transcription. Quantitative-rtPCR was performed to assess expression levels of target genes with
521 an Applied Biosystems (USA) QuantStudio 6 Flex instrument using SYBR Green reagent. Results were
522 normalized to *L32* expression, which was experimentally determined to not be differentially expressed
523 across diet and age cohorts. cDNA products were analyzed using the ΔC_T method. Primers used: *L32*
524 forward TCCACAATGTCAAGGAGCTG, reverse GGGATTGGTGACTCTGATGG; *Cidea* forward
525 TGCTCTTCTGTATCGCCCAGT, reverse GCCGTGTTAAGGAATCTGCTG; *Tbx1* forward
526 GGCAGGCAGACGAATGTTC, reverse TTGTCATCTACGGGCACAAAG; *Ucp1* forward
527 CCTCTCCAGTGGATGTGGTAA, reverse AGAAGCCACAAACCCTTTGA.

528

529 *Mitochondrial DNA quantification*

530 DNA was extracted from brown and inguinal adipose tissues using the Qiagen DNeasy Blood and
531 Tissue Kit. Briefly, 40mg of tissue was homogenized in 10% proteinase K through vortexing and
532 incubation at 56°C. DNA was precipitated with ethanol, collected in a spin column, and eluted in 150mL
533 of buffer. DNA concentration was quantified on a Nanodrop, and 50ng was used in a qPCR reaction to
534 quantify the amount of *h19* (nuclear gene) and *CytB* (mitochondrial gene). Mitochondrial content was

535 calculated as the ratio of mtDNA to nucDNA. Primers used: *Cytb* forward
536 TCTACGCTCAATCCCCAATAAAC, reverse TTAGGCTTCGTTGCTTTGAGGT; *h19* forward
537 TATGTGCCATTCTGCTGCGA, reverse AAGGTTTAGAGAGGGGGCCT.
538
539 *RNA sequencing and analyses*
540 Sixty-four LG/J and SM/J mice were used for sequencing analysis, representing 4 males and 4
541 females from each diet (high and low fat) and age (20 and 30 weeks). Total RNA was isolated from
542 interscapular brown and reproductive white adipose tissues using the RNeasy Lipid Tissue Kit (QIAgen).
543 RNA concentration was measured via Nanodrop and RNA quality/integrity was assessed with a
544 BioAnalyzer (Agilent). RNAseq libraries were constructed using the RiboZero kit (Illumina) from total RNA
545 samples with RIN scores >7.5. Libraries were checked for quality and concentration using the DNA
546 1000LabChip assay (Agilent) and quantitative PCR, according to manufacturer's protocol. Libraries were
547 sequenced at 2x100 paired end reads on an Illumina HiSeq 4000. After sequencing, reads were de-
548 multiplexed and assigned to individual samples.
549 FASTQ files were filtered to remove low quality reads and aligned against LG/J and SM/J custom
550 genomes using STAR (Dobin et al., 2013; Nikolskiy et al., 2015). Briefly, LG/J and SM/J indels and SNVs
551 were leveraged to construct strain-specific genomes using the GRC38.72-mm10 reference as a template.
552 This was done by replacing reference bases with alternative LG/J and SM/J bases using custom python
553 scripts. Ensembl R72 annotations were adjusted for indel-induced indexing differences for both genomes
554 (Macias-Velasco et al., 2019). Read counts were normalized via upper quartile normalization and a
555 minimum normalized read depth of 10 was required. Alignment summaries are provided in **Supplemental**
556 **Table 5 and Supplemental Figure 9**. Library complexity was assessed and differential expression
557 between each age cohort for each strain-by-diet comparison was determined after TMM normalization in
558 EdgeR (Chen et al., 2015) (**Supplemental Figure 10**).
559 Functional enrichment of differentially expressed genes was tested by over-representation
560 analysis in the WEB-based Gene Set Analysis Toolkit v2019 (Zhang et al., 2005). We performed analyses

561 of gene ontologies (biological process, cellular component, molecular function), pathway (KEGG), and
562 phenotype (Mammalian Phenotype Ontology). For each tissue, the list of all unique differentially
563 expressed genes was analyzed against the background of all unique genes expressed in that tissue
564 (Supplemental Tables 2 and 3). A Benjamini-Hochberg FDR-corrected p-value ≤ 0.05 was considered
565 significant.

566

567 *Correlation structure*

568 Co-expression was assessed for the set of 62 differentially expressed cytokines and ECM genes
569 by correlating expression of each gene with the expression of the other 61 genes in each diet-by-age
570 cohort. Each pair of genes then had their correlations correlated (R_g), where gene: G.

571 $$R_{g,G\in(i,j)} = cor\left(\begin{bmatrix} cor(G_i, G_1) \\ \vdots \\ cor(G_i, G_n) \end{bmatrix}, \begin{bmatrix} cor(G_j, G_1) \\ \vdots \\ cor(G_j, G_n) \end{bmatrix}\right)$$

572

573 Gene-pair-correlations were then compared between the high fat-fed 30 week-old cohort and the other
574 three cohorts (high fat-fed 30 weeks to high fat-fed 20 weeks, high fat-fed 30 weeks to low fat-fed 30
575 weeks, high fat-fed 30 weeks to low fat-fed 20 weeks) to obtain the ΔR_g between a pair of cohorts, where
576 cohort: K.

577 $$\Delta R_{g,G\in(i,j),K_1,K_2} = \left|R_{g,G\in(i,j),K_1} - R_{g,G\in(i,j),K_2}\right|$$

578

579 The median change in correlation ($M\Delta R_g$) was calculated and permutation was employed to identify the
580 background of expected $M\Delta R_g$ values. Permutation was performed by randomly selecting 2 groups of 8
581 animals from any cohort 10,000 times.

582 $$M\Delta R_{g,K_1,K_2} = median\left(\Delta R_{g,G\in(i,j),K_1,K_2}\right)$$

583

584 $M\Delta R_g$ was determined for the 2 randomized groups (rK_1, rK_2) for all 10,000 permutations to generate a
585 null model. Log transformation was performed to approximate normality, which was determined by Wilks-
586 Shapiro test and Q-Q plot. Significance was drawn from the cumulative normal null model to test if the
587 difference in correlation structure between each pair of cohorts was greater than by chance under the
588 randomized null model.

589 $$p_{K_1,K_2} = P\left(X \geq M\Delta R_{g,K_1,K_2}\right) \sim \mathcal{N}(\mu_r, \sigma_r)$$

590

591 *Brown adipose excision*

592 Interscapular brown adipose tissue depots were removed from 30 week-old high fat-fed SM/J
593 mice. A small longitudinal incision was made between the shoulder blades. All interscapular adipose
594 tissue was carefully removed, and a cauterizing wand used to stop excessive bleeding when necessary.
595 Surgeries were performed under general anesthesia by IP injection of ketamine/ xylazine (100/200
596 mg/Kg) and mice were maintained in the surgical plane by isofluorane/oxygen for the duration of the
597 procedure. Incisions were closed with 5-0 nonabsorbable sutures. Ketoprofen (2-5 mg/Kg) was provided
598 post-procedure and topical antibiotic was applied to the incision for up to 3 days as necessary. Animal
599 health and well-being was monitored daily. Sutures were removed at 10 days post-surgery. Four weeks
600 after surgery, mice underwent a glucose tolerance test and an insulin tolerance test one week later. After
601 an additional week of recovery, animals were sacrificed and serum and multiple tissues harvested
602 (reproductive and inguinal adipose depots, liver, heart, soleus, pancreas, hypothalamus) as described
603 above.

604

605 *Statistics*

606 Data within individual cohorts were assessed for normality using a Wilks-Shapiro test. Islet mass
607 and mitotic islet cell numbers were log10 transformed to achieve a normal distribution. Outliers were
608 identified by a Grubbs test ($p < 0.05$) and removed. Data were tested for significant differences among

609 cohorts by ANOVA with a Tukey's post-hoc correction. The sex-by-diet-by-age term was not significant
610 for any phenotype so males and females were pooled for analyses. P-values <0.05 were considered
611 significant. All statistical analyses were performed using the R software package.
612

613 **References**

614 Abdullah, A., Peeters, A., de Courten, M., and Stoelwinder, J. (2010). The magnitude of association
615 between overweight and obesity and the risk of diabetes: A meta-analysis of prospective cohort
616 studies. Diabetes Res. Clin. Pract.
617 Ahren, W. and (2004). The High-Fat Diet–Fed Mouse. Diabetes.
618 Beck, J.A., Lloyd, S., Hafezparast, M., Lennon-Pierce, M., Eppig, J.T., Festing, M.F.W., and Fisher,
619 E.M.C. (2000). Genealogies of mouse inbred strains. Nat. Genet.
620 CANNON, B. (2004). Brown Adipose Tissue: Function and Physiological Significance. Physiol. Rev.
621 Centers for Disease Control and Prevention (2017). National Diabetes Statistics Report. US Dep. Heal.
622 Hum. Serv.
623 Chatterjee, S., Khunti, K., and Davies, M.J. (2017). Type 2 diabetes. Lancet.
624 Chechi, K., Carpentier, A.C., and Richard, D. (2013). Understanding the brown adipocyte as a
625 contributor to energy homeostasis. Trends Endocrinol. Metab.
626 Chen, Y., Mccarthy, D., Robinson, M., and Smyth, G.K. (2015). edgeR : differential expression analysis
627 of digital gene expression data User's Guide.
628 Cheverud, J.M., Lawson, H.A., Fawcett, G.L., Wang, B., Pletscher, L.S., R Fox, A., Maxwell, T.J.,
629 Ehrich, T.H., Kenney-Hunt, J.P., Wolf, J.B., et al. (2011). Diet-dependent genetic and genomic
630 imprinting effects on obesity in mice. Obesity (Silver Spring). *19*, 160–170.
631 Chondronikola, M., Volpi, E., Børsheim, E., Porter, C., Annamalai, P., Enerbäck, S., Lidell, M.E., Saraf,
632 M.K., Labbe, S.M., Hurren, N.M., et al. (2014). Brown adipose tissue improves whole-body glucose
633 homeostasis and insulin sensitivity in humans. Diabetes.
634 Colditz, G.A., Willett, W.C., Rotnitzky, A., and Manson, J.E. (1995). Weight gain as a risk factor for

635 clinical diabetes mellitus in women. Ann. Intern. Med.
636 Cypess, A.M., Lehman, S., Williams, G., Tal, I., Rodman, D., Goldfine, A.B., Kuo, F.C., Palmer, E.L.,
637 Tseng, Y.-H., Doria, A., et al. (2009). Identification and importance of brown adipose tissue in adult
638 humans. N. Engl. J. Med. *360*, 1509–1517.
639 D'souza, A.M., Neumann, U.H., Glavas, M.M., and Kieffer, T.J. (2017). The glucoregulatory actions of
640 leptin. Mol. Metab.
641 Denroche, H.C., Kwon, M.M., Glavas, M.M., Tudurí, E., Philippe, M., Quong, W.L., and Kieffer, T.J.
642 (2016). The role of autonomic efferents and uncoupling protein 1 in the glucose-lowering effect of leptin
643 therapy. Mol. Metab.
644 Dobin, A., Davis, C.A., Schlesinger, F., Drenkow, J., Zaleski, C., Jha, S., Batut, P., Chaisson, M., and
645 Gingeras, T.R. (2013). STAR: ultrafast universal RNA-seq aligner. Bioinformatics *29*, 15–21.
646 Dulloo, A.G., and Montani, J.P. (2015). Pathways from dieting to weight regain, to obesity and to the
647 metabolic syndrome: An overview. Obes. Rev.
648 Edén, D., Siegbahn, A., and Mokhtari, D. (2015). Tissue factor/factor VIIa signalling promotes cytokine-
649 induced beta cell death and impairs glucose-stimulated insulin secretion from human pancreatic islets.
650 Diabetologia.
651 Ehrich, T.H., Kenney, J.P., Vaughn, T.T., Pletscher, L.S., and Cheverud, J.M. (2003). Diet, obesity, and
652 hyperglycemia in LG/J and SM/J mice. Obes. Res.
653 Flegal, K.M., Kruszon-Moran, D., Carroll, M.D., Fryar, C.D., and Ogden, C.L. (2016). Trends in Obesity
654 Among Adults in the United States, 2005 to 2014. JAMA *315*, 2284–2291.
655 Frantz, C., Stewart, K.M., and Weaver, V.M. (2010). The extracellular matrix at a glance. J. Cell Sci.
656 Gauger, K.J., Bassa, L.M., Henchey, E.M., Wyman, J., Bentley, B., Brown, M., Shimono, A., and
657 Schneider, S.S. (2013). Mice deficient in Sfrp1 exhibit increased adiposity, dysregulated glucose
658 metabolism, and enhanced macrophage infiltration. PLoS One.
659 Goossens, G.H. (2017). The Metabolic Phenotype in Obesity: Fat Mass, Body Fat Distribution, and
660 Adipose Tissue Function. Obes. Facts.

661 Gunawardana, S.C., and Piston, D.W. (2012). Reversal of type 1 diabetes in mice by brown adipose
662 tissue transplant. Diabetes.
663 Gunawardana, S.C., and Piston, D.W. (2015). Insulin-independent reversal of type 1 diabetes in
664 nonobese diabetic mice with brown adipose tissue transplant. Am. J. Physiol. Endocrinol. Metab. *308*,
665 E1043-55.
666 Hanssen, M.J.W., van der Lans, A.A.J.J., Brans, B., Hoeks, J., Jardon, K.M.C., Schaart, G., Mottaghy,
667 F.M., Schrauwen, P., van Marken Lichtenbelt, W.D., Lichtenbelt, W. van M., et al. (2016). Short-term
668 Cold Acclimation Recruits Brown Adipose Tissue in Obese Humans. Diabetes *65*, 1179–1189.
669 Hasegawa, Y., Ikeda, K., Chen, Y., Alba, D.L., Stifler, D., Shinoda, K., Hosono, T., Maretich, P., Yang,
670 Y., Ishigaki, Y., et al. (2018). Repression of Adipose Tissue Fibrosis through a PRDM16-GTF2IRD1
671 Complex Improves Systemic Glucose Homeostasis. Cell Metab.
672 Huang, G., Ge, G., Wang, D., Gopalakrishnan, B., Butz, D.H., Colman, R.J., Nagy, A., and Greenspan,
673 D.S. (2011). α3(V) Collagen is critical for glucose homeostasis in mice due to effects in pancreatic islets
674 and peripheral tissues. J. Clin. Invest.
675 Kahn, S.E., Prigeon, R.L., Schwartz, R.S., Fujimoto, W.Y., Knopp, R.H., Brunzell, J.D., and Porte, D.
676 (2001). Obesity, body fat distribution, insulin sensitivity and Islet beta-cell function as explanations for
677 metabolic diversity. J. Nutr.
678 Kajimura, S., Spiegelman, B.M., and Seale, P. (2015). Cell Metabolism Review Brown and Beige Fat:
679 Physiological Roles beyond Heat Generation. Cell Metab.
680 Karelis, A.D. (2008). Metabolically healthy but obese individuals. Lancet (London, England) *372*, 1281–
681 1283.
682 Kenchaiah, S., Evans, J.C., Levy, D., Wilson, P.W.F., Benjamin, E.J., Larson, M.G., Kannel, W.B., and
683 Vasan, R.S. (2002). Obesity and the Risk of Heart Failure. N. Engl. J. Med.
684 Kenney-Hunt, J.P., Vaughn, T.T., Pletscher, L.S., Peripato, A., Routman, E., Cothran, K., Durand, D.,
685 Norgard, E., Perel, C., and Cheverud, J.M. (2006). Quantitative trait loci for body size components in
686 mice. Mamm. Genome.

687 Kim, D., Kim, J., Yoon, J.H., Ghim, J., Yea, K., Song, P., Park, S., Lee, A., Hong, C.P., Jang, M.S., et
688 al. (2014). CXCL12 secreted from adipose tissue recruits macrophages and induces insulin resistance
689 in mice. Diabetologia.
690 Klöting, N., Fasshauer, M., Dietrich, A., Kovacs, P., Schön, M.R., Kern, M., Stumvoll, M., and Blüher,
691 M. (2010). Insulin-sensitive obesity. Am. J. Physiol. Metab.
692 Lagathu, C., Christodoulides, C., Tan, C.Y., Virtue, S., Laudes, M., Campbell, M., Ishikawa, K., Ortega,
693 F., Tinahones, F.J., Fernández-Real, J.M., et al. (2010). Secreted frizzled-related protein 1 regulates
694 adipose tissue expansion and is dysregulated in severe obesity. Int. J. Obes.
695 Lapa, C., Arias-Loza, P., Hayakawa, N., Wakabayashi, H., Werner, R.A., Chen, X., Shinaji, T.,
696 Herrmann, K., Pelzer, T., and Higuchi, T. (2017). Whitening and Impaired Glucose Utilization of Brown
697 Adipose Tissue in a Rat Model of Type 2 Diabetes Mellitus. Sci. Rep.
698 Lawson, H.A., and Cheverud, J.M. (2010). Metabolic syndrome components in murine models. Endocr.
699 Metab. Immune Disord. Drug Targets *10*, 25–40.
700 Lawson, H. a, Zelle, K.M., Fawcett, G.L., Wang, B., Pletscher, L.S., Maxwell, T.J., Ehrich, T.H.,
701 Kenney-Hunt, J.P., Wolf, J.B., Semenkovich, C.F., et al. (2010). Genetic, epigenetic, and gene-by-diet
702 interaction effects underlie variation in serum lipids in a LG/JxSM/J murine model. J. Lipid Res.
703 Lawson, H.A., Lee, A., Fawcett, G.L., Wang, B., Pletscher, L.S., Maxwell, T.J., Ehrich, T.H., Kenney-
704 Hunt, J.P., Wolf, J.B., Semenkovich, C.F., et al. (2011a). The importance of context to the genetic
705 architecture of diabetes-related traits is revealed in a genome-wide scan of a LG/J × SM/J murine
706 model. Mamm. Genome *22*, 197–208.
707 Lawson, H.A., Cady, J.E., Partridge, C., Wolf, J.B., Semenkovich, C.F., and Cheverud, J.M. (2011b).
708 Genetic effects at pleiotropic loci are context-dependent with consequences for the maintenance of
709 genetic variation in populations. PLoS Genet. *7*, e1002256.
710 Lawson, H.A., Zayed, M., Wayhart, J.P., Fabbrini, E., Love-Gregory, L., Klein, S., and Semenkovich,
711 C.F. (2017). Physiologic and genetic evidence links hemopexin to triglycerides in mice and humans. Int.
712 J. Obes. *41*.

713 Lee, J.T., Pamir, N., Liu, N.C., Kirk, E.A., Averill, M.M., Becker, L., Larson, I., Hagman, D.K., Foster-
714 Schubert, K.E., Van Yserloo, B., et al. (2014). Macrophage metalloelastase (MMP12) regulates adipose
715 tissue expansion, insulin sensitivity, and expression of inducible nitric oxide synthase. Endocrinology.
716 MacArthur, J.W. (2002). Genetics of Body Size and Related Characters. I. Selecting Small and Large
717 Races of the Laboratory Mouse. Am. Nat.
718 Macias-Velasco, J., St. Pierre, C., Wayhart, J., Yin, L., Spears, L., Miranda, M., Funai, K., Cheverud, J.,
719 Semenkovich, C., and Lawson HA (2019). Epistatic networks associated with parent-of-origin effects on
720 metabolic traits. BioRxiv.
721 Maquoi, E., Munaut, C., Colige, A., Collen, D., and Roger Lijnen, H. (2002). Modulation of adipose
722 tissue expression of murine matrix metalloproteinases and their tissue inhibitors with obesity. Diabetes.
723 van Marken Lichtenbelt, W.D., Vanhommerig, J.W., Smulders, N.M., Drossaerts, J.M.A.F.L., Kemerink,
724 G.J., Bouvy, N.D., Schrauwen, P., and Teule, G.J.J. (2009a). Cold-Activated Brown Adipose Tissue in
725 Healthy Men. N. Engl. J. Med.
726 van Marken Lichtenbelt, W.D., Vanhommerig, J.W., Smulders, N.M., Drossaerts, J.M.A.F.L., Kemerink,
727 G.J., Bouvy, N.D., Schrauwen, P., and Teule, G.J.J. (2009b). Cold-activated brown adipose tissue in
728 healthy men. N. Engl. J. Med.
729 Meigs, J.B., Wilson, P.W.F., Fox, C.S., Vasan, R.S., Nathan, D.M., Sullivan, L.M., and D'Agostino, R.B.
730 (2006). Body mass index, metabolic syndrome, and risk of type 2 diabetes or cardiovascular disease. J.
731 Clin. Endocrinol. Metab. *91*, 2906–2912.
732 Mejhert, N., Wilfling, F., Esteve, D., Galitzky, J., Pellegrinelli, V., Kolditz, C.I., Viguerie, N., Tordjman, J.,
733 Näslund, E., Trayhurn, P., et al. (2013). Semaphorin 3C is a novel adipokine linked to extracellular
734 matrix composition. Diabetologia.
735 Moreno-Viedma, V., Amor, M., Sarabi, A., Bilban, M., Staffler, G., Zeyda, M., and Stulnig, T.M. (2016a).
736 Common dysregulated pathways in obese adipose tissue and atherosclerosis. Cardiovasc. Diabetol.
737 Moreno-Viedma, V., Amor, M., Sarabi, A., Bilban, M., Staffler, G., Zeyda, M., and Stulnig, T.M. (2016b).
738 Common dysregulated pathways in obese adipose tissue and atherosclerosis. Cardiovasc. Diabetol.

739 Nathan, D.M., Barrett-Connor, E., Crandall, J.P., Edelstein, S.L., Goldberg, R.B., Horton, E.S., Knowler,
740 W.C., Mather, K.J., Orchard, T.J., Pi-Sunyer, X., et al. (2015). Long-term effects of lifestyle intervention
741 or metformin on diabetes development and microvascular complications over 15-year follow-up: The
742 Diabetes Prevention Program Outcomes Study. Lancet Diabetes Endocrinol.
743 Nikolskiy, I., Conrad, D.F., Chun, S., Fay, J.C., Cheverud, J.M., and Lawson, H.A. (2015). Using whole-
744 genome sequences of the LG/J and SM/J inbred mouse strains to prioritize quantitative trait genes and
745 nucleotides. BMC Genomics *16*, 415.
746 Norgard, E.A., Lawson, H.A., Pletscher, L.S., Wang, B., Brooks, V.R., Wolf, J.B., and Cheverud, J.M.
747 (2011). Genetic factors and diet affect long-bone length in the F34 LG,SM advanced intercross. Mamm.
748 Genome *22*, 178–196.
749 Ouellet, V., Labbé, S.M., Blondin, D.P., Phoenix, S., Guérin, B., Haman, F., Turcotte, E.E., Richard, D.,
750 and Carpentier, A.C. (2012). Brown adipose tissue oxidative metabolism contributes to energy
751 expenditure during acute cold exposure in humans. J. Clin. Invest.
752 Poekes, L., Lanthier, N., and Leclercq, I.A. (2015). Brown adipose tissue: a potential target in the fight
753 against obesity and the metabolic syndrome. Clin. Sci.
754 Rauscher, G.H., Mayne, S.T., and Janerich, D.T. (2000). Relation between body mass index and lung
755 cancer risk in men and women never and former smokers. Am. J. Epidemiol.
756 Raz, V., Sterrenburg, E., Routledge, S., Venema, A., van der Sluijs, B.M., Trollet, C., Dickson, G., van
757 Engelen, B.G.M., van der Maarel, S.M., and Antoniou, M.N. (2013). Nuclear entrapment and
758 extracellular depletion of PCOLCE is associated with muscle degeneration in oculopharyngeal
759 muscular dystrophy. BMC Neurol.
760 Reeves, G.K., Pirie, K., Beral, V., Green, J., Spencer, E., and Bull, D. (2007). Cancer incidence and
761 mortality in relation to body mass index in the Million Women Study: Cohort study. Br. Med. J.
762 Roat, R., Rao, V., Doliba, N.M., Matschinsky, F.M., Tobias, J.W., Garcia, E., Ahima, R.S., and Imai, Y.
763 (2014). Alterations of pancreatic islet structure, metabolism and gene expression in diet-induced obese
764 C57BL/6J mice. PLoS One.

765 Roberts-Toler, C., O'Neill, B.T., and Cypess, A.M. (2015). Diet-induced obesity causes insulin
766 resistance in mouse brown adipose tissue. Obesity.
767 Rosen, E.D., and Spiegelman, B.M. (2014). What we talk about when we talk about fat. Cell.
768 Saito, M. (2013). Brown adipose tissue as a regulator of energy expenditure and body fat in humans.
769 Diabetes Metab. J.
770 Saito, M., Okamatsu-Ogura, Y., Matsushita, M., Watanabe, K., Yoneshiro, T., Nio-Kobayashi, J.,
771 Iwanaga, T., Miyagawa, M., Kameya, T., Nakada, K., et al. (2009). High incidence of metabolically
772 active brown adipose tissue in healthy adult humans: Effects of cold exposure and adiposity. Diabetes.
773 Shimizu, I., and Walsh, K. (2015). The Whitening of Brown Fat and Its Implications for Weight
774 Management in Obesity. Curr. Obes. Rep.
775 Shimizu, I., Aprahamian, T., Kikuchi, R., Shimizu, A., Papanicolaou, K.N., MacLauchlan, S., Maruyama,
776 S., and Walsh, K. (2014). Vascular rarefaction mediates whitening of brown fat in obesity. J. Clin.
777 Invest.
778 Shu, L., Chan, K.H.K., Zhang, G., Huan, T., Kurt, Z., Zhao, Y., Codoni, V., Trégouët, D.A., Yang, J.,
779 Wilson, J.G., et al. (2017). Shared genetic regulatory networks for cardiovascular disease and type 2
780 diabetes in multiple populations of diverse ethnicities in the United States. PLoS Genet.
781 Da Silva Xavier, G. (2018). The Cells of the Islets of Langerhans. J. Clin. Med.
782 Skrbic, B., Engebretsen, K.V.T., Strand, M.E., Lunde, I.G., Herum, K.M., Marstein, H.S., Sjaastad, I.,
783 Lunde, P.K., Carlson, C.R., Christensen, G., et al. (2015). Lack of collagen VIII reduces fibrosis and
784 promotes early mortality and cardiac dilatation in pressure overload in mice. Cardiovasc. Res.
785 Stanford, K.I., Middelbeek, R.J.W., Townsend, K.L., An, D., Nygaard, E.B., Hitchcox, K.M., Markan,
786 K.R., Nakano, K., Hirshman, M.F., Tseng, Y.-H., et al. (2013). Brown adipose tissue regulates glucose
787 homeostasis and insulin sensitivity. J. Clin. Invest. *123*, 215–223.
788 Strazzullo, P., D'Elia, L., Cairella, G., Garbagnati, F., Cappuccio, F.P., and Scalfi, L. (2010). Excess
789 body weight and incidence of stroke: Meta-analysis of prospective studies with 2 million participants.
790 Stroke.

791 Sun, K., Tordjman, J., Clément, K., and Scherer, P.E. (2013). Fibrosis and adipose tissue dysfunction.
792 Cell Metab.
793 Takahashi, N., Yoshizaki, T., Hiranaka, N., Kumano, O., Suzuki, T., Akanuma, M., Yui, T., Kanazawa,
794 K., Yoshida, M., Naito, S., et al. (2015). The production of coagulation factor VII by adipocytes is
795 enhanced by tumor necrosis factor-α or isoproterenol. Int. J. Obes.
796 Tomiyama, A.J., Ahlstrom, B., and Mann, T. (2013). Long-term Effects of Dieting: Is Weight Loss
797 Related to Health? Soc. Personal. Psychol. Compass.
798 Villarroya, F., Cereijo, R., Villarroya, J., and Giralt, M. (2017). Brown adipose tissue as a secretory
799 organ. Nat. Rev. Endocrinol.
800 Virtanen, K.A., Lidell, M.E., Orava, J., Heglind, M., Westergren, R., Niemi, T., Taittonen, M., Laine, J.,
801 Savisto, N.-J., Enerbäck, S., et al. (2009). Functional Brown Adipose Tissue in Healthy Adults. N. Engl.
802 J. Med.
803 Wang, G.-X., Zhao, X.-Y., Meng, Z.-X., Kern, M., Dietrich, A., Chen, Z., Cozacov, Z., Zhou, D.,
804 Okunade, A.L., Su, X., et al. (2014). The brown fat-enriched secreted factor Nrg4 preserves metabolic
805 homeostasis through attenuation of hepatic lipogenesis. Nat. Med. *20*, 1436–1443.
806 Wang, G.X., Zhao, X.Y., and Lin, J.D. (2015). The brown fat secretome: Metabolic functions beyond
807 thermogenesis. Trends Endocrinol. Metab.
808 Wu, J., Boström, P., Sparks, L.M., Ye, L., Choi, J.H., Giang, A.H., Khandekar, M., Virtanen, K.A.,
809 Nuutila, P., Schaart, G., et al. (2012). Beige adipocytes are a distinct type of thermogenic fat cell in
810 mouse and human. Cell.
811 Yang, W., Dall, T.M., Beronjia, K., Lin, J., Semilla, A.P., Chakrabarti, R., Hogan, P.F., and Petersen,
812 M.P. (2018). Economic costs of diabetes in the U.S. in 2017. Diabetes Care.
813 Zhang, B., Kirov, S., and Snoddy, J. (2005). WebGestalt: An integrated system for exploring gene sets
814 in various biological contexts. Nucleic Acids Res.
815
816

817 **List of Supplementary Figures:**

818 **Supplemental Figure 1:** Physiological parameters of the LG/J inbred mouse strain.

819 **Supplemental Figure 2:** Pancreatic islet phenotypes and additional cell quantification

820 **Supplemental Figure 3:** Brown adipose tissue quantification of LG/J mice.

821 **Supplemental Figure 4:** SM/J adipose histology

822 **Supplemental Figure 5:** SM/J thermogenic parameters

823 **Supplemental Figure 6:** Differential expression by age in LG/J cohorts

824 **Supplemental Figure 7:** Eight cytokine and extracellular matrix genes differentially expressed in SM/J

825 high fat brown adipose between 20 and 30 weeks

826 **Supplemental Figure 8:** STAR alignment summaries for RNA-sequencing results

827 **Supplemental Figure 9:** Common and tagwise dispersion of RNA sequencing cohorts.

828

829 **List of Supplementary Tables:**

830 **Supplemental Table 1:** High and low fat diet constituents.

831 **Supplemental Table 2:** Differential expression results in SM/J mice.

832 **Supplemental Table 3:** Differential expression results in LG/J mice.

833 **Supplemental Table 4:** Overrepresentation analysis results for SM/J BAT.

834 **Supplemental Table 5:** STAR alignment summaries for RNA-sequencing results.

835

836 **RNA sequencing count data available for download at:** http://lawsonlab.wustl.edu/data/